NONLINEAR ESTIMATORS FOR OBTAINING ANALYTICAL REDUNDANCY OF THE AERODYNAMIC STATES

W. Dunkel
Technical University of Braunschweig
Institute for Flight Guidance and Control
Rebenring 18, D-38106 Braunschweig
Germany

Abstract

A nonlinear deterministic observer and a recursive equation solver are described for obtaining analytic and dissimilar redundancy of primary sensors. Both approaches use the nonlinear relationship between measurements of the inertial navigation system INS (namely the measured accelerations and angular velocities) to determine the airspeed, the angle of attack and the angle of sideslip with high accuracy. To decrease the influence of wind disturbances a model of the aircraft specific aerodynamic and propulsion system are used rather than a kinematic model. This application was tested using a small transportation aircraft with two turboprop engines and STOL facilities.

This paper discusses both the improvements of the needed aircraft model by a Maximum-Likelihood off-line identification as well as the design of the estimators. The main emphasis is the improvement of the process model and the model of the measurement system through the use of additional sensors. The data compatibility check can be improved by using the very precise GPS satellite navigation system in differential mode (DGPS) to obtain more precise measurement correction values and a more precise estimation of the wind disturbances. To decrease the correlation of drag and thrust as well as lift and earth mass attraction a Pitot tube is placed behind the propeller for thrust estimation and differential pressure sensors are placed in the wing for lift estimation.

1 Introduction

In civil aircraft, estimator are used mainly in navigation systems. It has been shown using experimental aircraft that estimators can also be used to obtain additional analytic and dissimilar redundancy for the supervision of primary sensors. Sensor supervision systems mostly use parameter identification methods based on Kalman filters / 11/ and kinematic aircraft models / 16/. The model based supervision of sensors discussed here employs an observer for state estimation. The function of such a system, as well as first experimental results, were presented in / 7/, / 8/. This paper discusses recent improvements of the estimation using improved models and better estimators.

One particularly interesting aircraft application of this estimation is the supervision of aerodynamic states as demonstrated by the aircraft velocity $\underline{V}_A$ with the airspeed V_A the angle of attack α and the angle of sideslip β. For the use of a kinematic model (estimation of the flight-path velocity $\underline{V}_K$), the aircraft velocity $\underline{V}_A$ can neither be measured independently of the wind velocity $\underline{V}_W$ nor is a universally valid model available for the estimation of wind. To avoid such problems, the presented method uses the other part of the aircraft model, namely the aircraft specific equations of the aerodynamic force $\underline{R}^A$ and the propeller force $\underline{R}^F$ (Fig. 1). The nonlinear relationship of the acceleration $\underline{a}$ and the aircraft velocity $\underline{V}_A$) allows one, dependent on the employed estimation method and the complexity of the implemented model, to dramatically reduce the influence of wind.

The main goal of the paper is to present two implementations of analytic redundancy for the supervision of a ROSEMOUNT five hole probe. The design and the discussion of a nonlinear observer and a

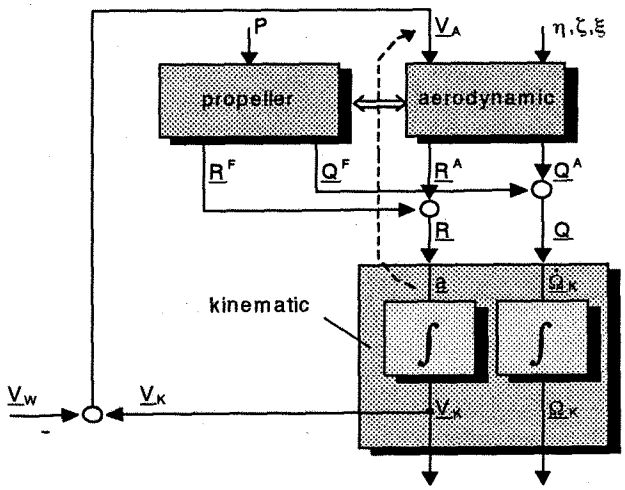

Fig. 1: Block diagram of a portion of the aircraft model (with: shaft power P, moment Q).

nonlinear recursive equation solver are described and the results are compared. To obtain the required accuracy, both discussed approaches are based on the same underlying simple but precise model.

The most effort will therefore be devoted to the improvement of this model. Therefore a system identification approach was taken using the research aircraft DORNIER DO128 equipped with advanced measurement equipment. In the first step of the off-line identification, the well-known differential equations of the kinematic airplane model are used to estimate the unknown parameters of the extended measurement model. This data compatibility check (also called flight path reconstruction / 18/) additionally uses GPS (Global Positioning System) satellite navigation data. In differential mode (DGPS), positions are determined with an uncertainty of about one meter / 23/. This positional information can be used to improve the measurement model and the estimation of the wind disturbances. The second step of the identification uses propulsion system and aerodynamic models to estimate the unknown aircraft-specific parameters, especially the force coefficients of the aerodynamics.

So far the major problem of this step has been the lack of experimental data to separate the effects of the coupled aerodynamic and propeller processes. The output quantities forces $\underline{R}^A$, $\underline{R}^F$ and moments $\underline{Q}^A$, $\underline{Q}^F$ are not measurable. Using the standard aircraft equipment (the laser strapdown platform of the INS) the measurable quantities closest related to these variables are the acceleration $\underline{a}$ and the angular velocity $\underline{\Omega}_K$ (block „kinematic" in Fig. 1)

To obtain additional quantities for the identification,

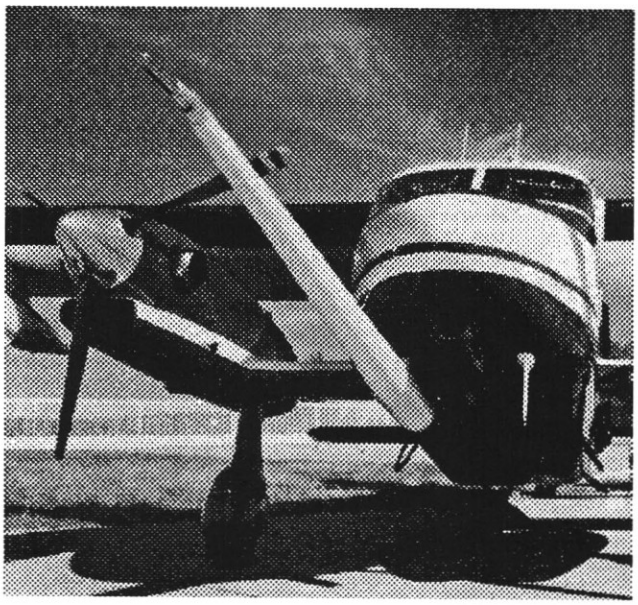

Fig. 2: The research aircraft DORNIER DO128-6 a small STOL transport aircraft with 2 turboprop engines (weight: 4t).

the research aircraft shown in Fig. 2 was equipped with an additional Pitot tube Fig. 10 located behind the right propeller. Using the Pitot tube the additional stream velocity, which is a function of the thrust, can be measured.

The installation of four supplementary pressure sensors in the wing allow one to determine additionally the pressure in two wing sections. Two differential pressure sensors are placed in the wing section behind the propeller for measuring the pressure between the upper (lower) surface of the wing and the static pressure. The remaining two sensors are placed in a wing section outside the propeller stream (and the aileron).

These additional measurements will result in an improved model for both estimators with dramatically reduced estimation error. For standard flight conditions, an estimation accuracy comparable to the angles α, β of less than 0.2 degrees and comparable to the airspeed V_A of less than 0.5m/s is expected. This estimator accuracy is required for implementation of analytic redundancy (estimator) and fault detection (e.g. in combination with the pattern recognition algorithm from Ref. / 5/) in a standard aircraft.

2 Identification

In this off-line application a Maximum-Likelihood output error algorithm is used to estimate the unknown parameters of the process. For this reason only constant parameters can be estimated and process noise is neglected.

The identification is preferably done in two main steps according to the "Estimation Before Modeling" technique / 19/. In a first step the well-known differential equations of the kinematic airplane model are used to estimate both the unknown parameters of the measurement system and the quasi static wind model (Section 2.1). In the second step a propeller model and an aerodynamic model are used to estimate the unknown aircraft-specific parameters (Section 2.2). Advanced sensor systems allow to improve both parts of the model.

2.1 Data Compatibility Check

The compatibility check is the first step of the identification. It ensures that the measurements used in later identification steps are consistent and effectively error-free. For the compatibility check the flight-path velocity, the position vector and the vector of the Euler angles are estimated by integrating the measured body-fixed accelerations and angular velocities. Comparing the 12 estimated and measured output variables (Φ, Θ, Ψ, V_{GS}, χ, $\dot{h}$, φ, λ, h, $\bar{q}$, p_α, p_β) the measurement corrections (bias, scaling factors, time shifts) and other parameters can be estimated. This requires that the data contains the

necessary movements to sufficiently constrain these parameter estimates.

2.1.1 Improvements by DGPS Data

The improved data compatibility check presented here makes use of the satellite navigation system (Global Positioning System, GPS) with its main output quantities latitude, longitude and altitude. In differential mode (DGPS) positions are determined with an uncertainty of about one meter (valid for low dynamic maneuvers). If the model is extended accordingly, this DGPS-data can be used to improve the accuracy of the measurement check (e.g., the estimation of the wind disturbances).

Positions determined using GPS satellites are sensitive to the satellite configuration, the current atmospheric conditions, and other factors. The idea of DGPS is to correct the on-board recorded GPS satellite raw data with the data of a ground station. The nearby ground station (in our application less than 100km away) has a well known or very precise computable position and can determine corrections for GPS raw data recorded on-board the aircraft. These position corrections are combined in an off-line computation (in this application).

Fig. 3 compares the data of INS/airdata, the computed data of the SERCHEL NR103-GPS receiver located on board the aircraft, and the off-line calculated DGPS from satellite raw data. It is obvious from this comparison that DGPS yields the best positional information. INS output has a current offset of about 1.8 [km] as well as a drift, and GPS has only a position accuracy of about 100m. Remarkable is the difference of the three output signals of the altitude 'h'. The barometric altitude (airdata) is calculated from the static pressure and is influenced by aircraft maneuvers and the current atmospheric conditions. The difference between GPS computed data and DGPS results from different coordinate systems. Both are based on the WGS84 (Fig. 4) but the GPS receiver additionally uses geoid corrections which results in a difference of 80 [m] for the current longitude and latitude. In addition the GPS receiver has a jump in the computed altitude (reconfiguration mode of the receiver).

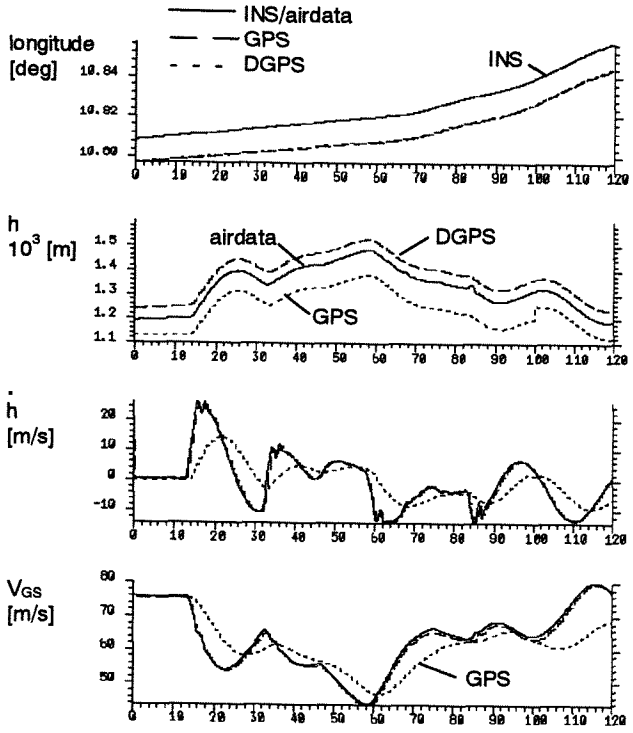

Fig. 3: Comparison of INS/airdata, GPS and DGPS.

It is not a good idea to choose GPS computed data to determine the flight-path velocity although these signals are available. From Fig. 3 one can conclude that the receiver has a strong low pass filter in its velocity outputs (time constant about 6s). The calculated DGPS signal is influenced by errors coming from the more or the less bad dynamic behavior of the receiver's HF-part. Hence, the following data compatibility check uses the DGPS signals for positional information and the INS signals for the determination of the flight-path velocity.

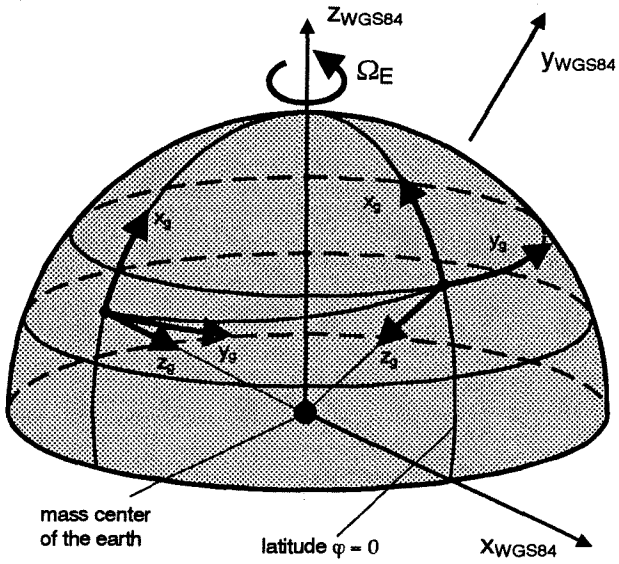

Fig. 4 The Word Geodetic System WGS84.

So far the data compatibility check models /8/, /14/, /18/, /19/, /22/ considered the earth as a flat non-rotating system. To obtain the required position accuracy for the identification model the equations now have to be expanded to the description of the earth as a rotating ellipsoid. Hence, the earth is described in the WGS84 coordinate system (Word Geodetic System from 1984, here without geoid corrections, Fig. 4) / 24/ and the kinematic model is extended to estimate all elements of the position vector.

2.1.2 The Kinematic Model

The measured angular velocity $\underline{\Omega}_b^{ib}$ (between inertial- and body axis system: index superscript „ib", measured in body-fixed coordinates: index subscript „b") is measured by laser gyros. This velocity includes the angular velocity between the inertial system and the earth-fixed (WGS84) coordinate system $\underline{\Omega}_g^{ie}$

$$\underline{\Omega}_g^{ie} = \left[\Omega_E \cdot \cos\varphi, \quad 0, \quad -\Omega_E \cdot \sin\varphi\right]_g^T \qquad (1)$$

and the angular velocity between earth-fixed and geodetic coordinate system $\underline{\Omega}_g^{eg}$

$$\underline{\Omega}_g^{eg} = \left[\dot{\lambda} \cdot \cos\varphi, \quad -\dot{\varphi}, \quad -\dot{\lambda} \cdot \sin\varphi\right]_g^T \quad . \qquad (2)$$

The rotation speed of the earth can be found to be $\Omega_E = 7292115 \cdot 10^{-11} \text{rad s}^{-1}$ / 24/.

The transformation matrix $\underline{\underline{M}}_{bg}$ from geodetic to body-fixed coordinates (a function of the Euler angles) leads to $\underline{\Omega}_b^{gb}$ and to the differential equation for determining the vector of the Euler angles $\underline{\Phi} = \left[\Phi, \quad \Theta, \quad \Psi\right]^T$ with the bank angle (roll angle) Φ, the inclination angle (pitch angle) Θ and the azimuth angle (yaw angle) Ψ

$$\partial\underline{\Phi} / \partial t = \underline{\Omega}_b^{gb} = \underline{\Omega}_b^{ib} - \underline{\underline{M}}_{bg} \cdot (\underline{\Omega}_g^{ie} + \underline{\Omega}_g^{eg}) \quad . \qquad (3)$$

The acceleration which can be measured in the aircraft's center of gravity $\underline{a}_b^{ib}$ includes the acceleration from earth mass attraction $\underline{G}_g$, centripetal $\underline{\Omega}_g^{ie} \times (\underline{\Omega}_g^{ie} \times \underline{r}_g)$ and Coriolis acceleration. Therefore the vector differential equation of the transport acceleration $\partial\underline{V}_{Kg}/\partial t$ can be written as

$$\begin{aligned} \partial\underline{V}_{Kg} / \partial t = {} & \underline{\underline{M}}_{gb} \cdot \underline{a}_b^{ib} + \underline{G}_g - \underline{\Omega}_g^{ie} \times (\underline{\Omega}_g^{ie} \times \underline{r}_g) \\ & - 2\underline{\Omega}_g^{ie} \times \underline{V}_{Kg} - \underline{\Omega}_g^{eg} \times \underline{V}_{Kg} \end{aligned} \qquad (4)$$

with the earth mass attraction (the earth's gravitational constant μ=0.039860015 [m^3/s^2] / 24/)

$$\underline{G}_g = \left[0, \quad 0, \quad \frac{\mu}{(R_M + h)^2}\right]_g^T \quad , \qquad (5)$$

and the radius vector from the middle of the earth to the aircraft's center of gravity

$$\underline{r}_g = \left[0, \quad 0, \quad R_M + h\right]_g^T \quad . \qquad (6)$$

This leads to the transport velocity in Cartesian coordinates $\underline{V}_{Kg} = \left[u_K, \quad v_K, \quad w_K\right]_g^T$.

The position of the aircraft in earth-fixed coordinates (latitude φ, longitude λ, altitude h) can be obtained by the following differential equations

$$\partial\varphi / \partial t = \frac{u_{Kg}}{(R_M + h)} \qquad (7)$$

$$\partial\lambda / \partial t = \frac{v_{Kg}}{(R_M + h) \cdot \cos\varphi} \qquad (8)$$

$$\partial h / \partial t = -w_{Kg} \quad . \qquad (9)$$

The still unknown quantities in (5), (6), (7) and (8) are the local earth's meridian radius of curvature R_M and the local earth's transverse radius of curvature R_P. With the earth's semimajor axis a=6378145 [m] and the first eccentricity of the earth e=0.0818191908426 / 24/ R_M and R_P are given by

$$R_M = \frac{a \cdot (1 - e^2)}{\sqrt[3]{1 - e^2 \sin^2\varphi}} \qquad (10)$$

$$R_P = \frac{a}{\sqrt{1 - e^2 \sin^2\varphi}} \quad . \qquad (11)$$

2.1.3 The Wind Model

So far the flight-path velocity is estimated and its corrections can be obtained by the identification. To correct the measured aircraft velocity the wind velocity is needed, too

$$\underline{V}_A = \underline{V}_K - \underline{V}_W \quad . \qquad (12)$$

Since the flight tests were carried out during non-turbulent weather conditions the influence of high-frequency turbulence is negligible. However, low frequent wind effects must be taken into account because of their direct influence on the accuracy of the aircraft velocity estimation. For example the zero shift of the angle of attack $\Delta\alpha$ is besides others correlated with wind speeds u_W and w_W

$$\alpha = k_\alpha \cdot \alpha^m + \Delta\alpha = \arctan\frac{w_A}{u_A} = \arctan\frac{w_K - w_W}{u_K - u_W} \quad . \qquad (13)$$

The wind is approximated by a quasi static geodetic wind field (typically 4x4 km base) modeled by Chebychev polynomials / 17/. The wind in each direction is a third order function of the current aircraft's geodetic position $\underline{r}_g$ $\underline{r}_g = \left[x, \quad y, \quad z\right]_g^T$ (with $\dot{\underline{r}}_g = \underline{V}_{Kg}$ and initial condition $\underline{r}_g(t = 0) = \underline{0}$) in each of the tree possible directions.

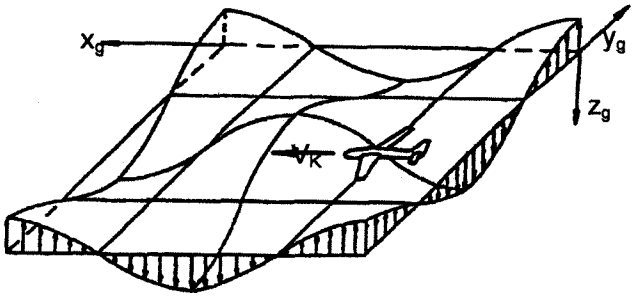

Fig. 5: A possible vertical wind w_{Wg}-distribution (here at a constant altitude h) / 2/

$$\underline{V}_{Wg} = \left[u_W \quad v_W \quad w_W\right]_g^T \tag{14}$$

$$\underline{V}_{Wg} = \begin{bmatrix} u_{W0} + \sum_{n=1}^{3} u_{Wx^n} \cdot x^n + \sum_{n=1}^{3} u_{Wy^n} \cdot y^n + \sum_{n=1}^{3} u_{Wz^n} \cdot z^n \\ v_{W0} + \sum_{n=1}^{3} v_{Wx^n} \cdot x^n + \sum_{n=1}^{3} v_{Wy^n} \cdot y^n + \sum_{n=1}^{3} v_{Wz^n} \cdot z^n \\ w_{W0} + \sum_{n=1}^{3} w_{Wx^n} \cdot x^n + \sum_{n=1}^{3} w_{Wy^n} \cdot y^n + \sum_{n=1}^{3} w_{Wz^n} \cdot z^n \end{bmatrix} \tag{15}$$

The approximation of the wind is very good due to the improved accuracy of the estimated position (by the use of DGPS) and the improved determination of the flight-path velocity. In Fig. 6 the estimated wind along the flight-path is compared with the on-board calculated wind / 21/ which is not an observation quantity in the identification. Differences can be rationalized by considering the limitations of polynomial approximation (third order max., in Fig. 6 u_W and v_W are only first order) and by the errors of the

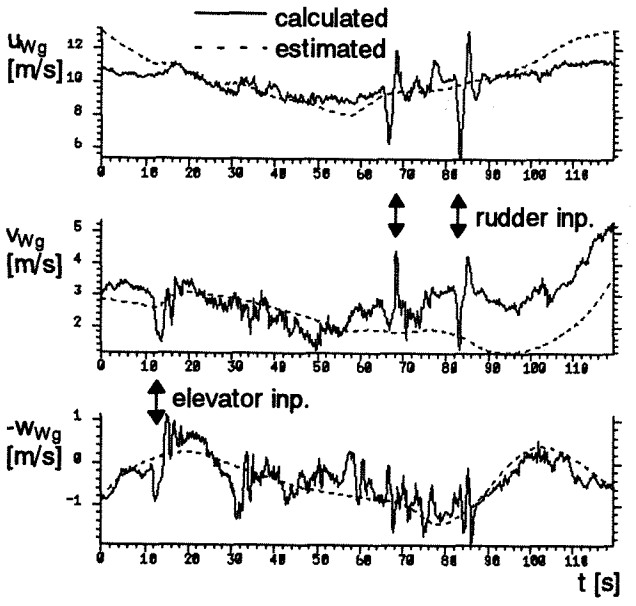

Fig. 6: Identification results of the wind estimation.

on-board wind calculation (correlation with the input signals, sensor errors).

For this estimated wind velocity (Fig. 6) the estimation of the pressures at the five hole probe (function of the aircraft velocity) is presented in Fig. 9.

2.1.4 The Measurement Equations

As mentioned before all measurements of the process (inputs $\underline{u}$ and outputs $\underline{y}$) are assumed to be affected by bias Δu, Δy and scaling factors k_u, k_y

$$u_i = k_{ui} \cdot u_i + \Delta u_i \tag{16}$$

$$y_j = k_{yj} \cdot y_j + \Delta y_j \tag{17}$$

as well as time shifts relative to the time shift of the angular velocities (reference). The necessary time shifts are archived by the estimation of time constants T of a PT_1 (a linear first order lag)

$$\dot{y}_{tj} = (y_j - y_{tj}) / T_j \quad ; \; y_{tj}(t_0) = y_j(t_0) \; . \tag{18}$$

If the estimated time constant T is less than $(2/3)\cdot\Delta T$ or larger than $2\cdot\Delta T$ the delay is shifted into an integer multiple l of the time step ΔT

$$y_j(t) = y_j(t + l_{\tau y_j} \cdot \Delta T) \; . \tag{19}$$

Thus, the damping of higher frequency signal amplitudes does not increase excessively / 12/.

In addition to the discussed common measurement corrections there are additional measurement equations for the input signals (especially the acceleration) and some of the output variables to consider.

2.1.4.1 Measurement of the Acceleration

The acceleration normally cannot be measured in the aircraft's center of gravity. The center of gravity is not constant because of the fuel consumption. The distance from the center of gravity to the accelerometers $\underline{X}_b^{acc}$ must be taken into account

$$\underline{a}_b^{ib} = \underline{a}_b^m - \underline{\Omega}_b^{gb} \times \left[\dot{\underline{X}}_b^{acc} + \underline{\Omega}_b^{gb} \times \underline{X}_b^{acc}\right] - \dot{\underline{\Omega}}_b^{gb} \times \underline{X}_b^{acc} \; . \tag{20}$$

Normally the variation of the distance, caused for example by fuel consumption, is negligible $\dot{\underline{X}}_b^m \approx 0$.

2.1.4.2 Measurement of the Flight-Path Velocity

With (4) the observation equations of the ground speed V_{GS} and the true track χ are

$$V_{GS} = \sqrt{u_{Kg}^2 + v_{Kg}^2} \tag{21}$$

$$\chi = \arctan(v_{Kg} / u_{Kg}) \; . \tag{22}$$

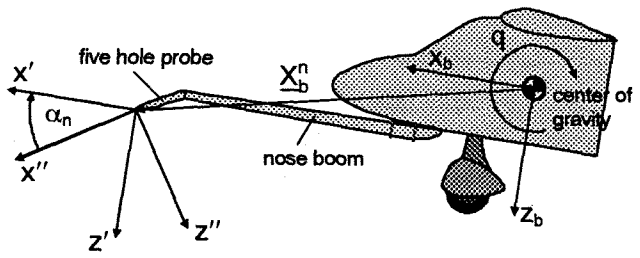

Fig. 7: Geometry of the transformation procedure into the axis system of the five hole probe (2D illustration, xz-plane, β_n=0).

2.1.4.3 Pressures at the Five Hole Probe

The aircraft velocity is the difference between flight path velocity and wind velocity (12). Derived from the aircraft velocity the differential pressures at the tip of the nose-boom (with the five hole probe) are calculated as illustrated in Fig. 7.

The wind velocity at the tip of the nose-boom described in geodetic coordinates $\underline{V}'_{Wg}$ is calculated according (15). The position within the wind field is given by the position of the aircraft's center of gravity $\underline{X}_g^{cg}$ in geodetic coordinates plus the distance between the center of gravity and the tip of the noseboom $\underline{X}_b^n$ which is given in the body-fixed coordinates and has to be transformed into geodetic coordinates.

$$\underline{V}'_{Wg} = \underline{V}_{Wg}\Big|_{(\underline{X}_g^{cg} + \underline{\underline{M}}_{gb}\underline{X}_b^n)} \quad . \tag{23}$$

The aircraft velocity at the tip of the nose-boom $\underline{V}'_A$ is the difference between the aircraft velocity in the center of gravity $\underline{V}_{Kg}$ transformed into body-fixed coordinates plus the additional speed at the tip of the nose-boom by the rotation of the aircraft $\underline{\Omega}_b^{gb} \times \underline{X}_b^n$ and the wind velocity in body-fixed coordinates

$$\underline{V}'_A = \underline{\underline{M}}_{bg} \cdot \underline{V}_{Kg} + \underline{\Omega}_b^{gb} \times \underline{X}_b^n - \underline{\underline{M}}_{bg} \cdot \underline{V}'_{Wg} \quad . \tag{24}$$

From (24) the components of the aircraft velocity in Cartesian body-fixed coordinates at the tip of the nose-boom can be calculated by

$$V'_A = \sqrt{u'^2_A + v'^2_A + w'^2_A} \tag{25}$$

$$\alpha' = \arctan\frac{w'_A}{u'_A} \tag{26}$$

$$\beta' = \arcsin\frac{v'_A}{\sqrt{u'^2_A + v'^2_A + w'^2_A}} \quad . \tag{27}$$

To obtain the pressures measured at the five hole probe the aircraft velocity (24) has to be transformed into the rotated coordinate system of this sensor.

$$\begin{bmatrix} u''_A \\ v''_A \\ w''_A \end{bmatrix} = \begin{bmatrix} \cos\alpha_n \cos\beta_n & -\cos\alpha_n \sin\beta_n & -\sin\alpha_n \\ \sin\beta_n & \cos\beta_n & 0 \\ \sin\alpha_n \cos\beta_n & -\sin\alpha_n \sin\beta_n & \cos\alpha_n \end{bmatrix} \cdot \begin{bmatrix} u'_A \\ v'_A \\ w'_A \end{bmatrix} \tag{28}$$

The x-direction of this coordinate system x" is given by the longitudinal axis of the five hole probe (see Fig. 7). The rotation angles are $\alpha_n \approx 7°$ and $\beta_n \approx 0°$. For β_n=0° the Equ. (28) is simplified to

$$\begin{bmatrix} u''_A \\ v''_A \\ w''_A \end{bmatrix} = \begin{bmatrix} \cos\alpha_n & 0 & -\sin\alpha_n \\ 0 & 1 & 0 \\ \sin\alpha_n & 0 & \cos\alpha_n \end{bmatrix} \cdot \begin{bmatrix} u'_A \\ v'_A \\ w'_A \end{bmatrix} \quad . \tag{29}$$

The differential pressures of the five hole probe are then obtained according to / 6/. In the special case of the ROSEMOUNT five hole probe the diameter of the center hole for the measurement of the dynamic pressure is larger than the four other holes (45 [°]) and it is large compared to the diameter of the hemisphere at the tip.

So the single parameter in the model used in Ref. / 6/ is now separated into two form parameters b_1 for the determination of non-axial flow and b_2 for axial flow. It is expected that the estimated parameter b_2 will always be nearly zero.

$$\bar{q} = p_t - p_s = \frac{\rho}{2} \cdot \left(u''^2_A + (1 - b_2) \cdot (v''^2_A + w''^2_A) \right) \tag{30}$$

$$p_\alpha = \rho \cdot b_1 \cdot u''_A \cdot w''_A \tag{31}$$

$$p_\beta = \rho \cdot b_1 \cdot u''_A \cdot v''_A \quad . \tag{32}$$

In (30) $\bar{q}$ is the dynamic pressure, p_α and p_β in (31) and (32) are the differential pressures in z" and y" direction. The air density ρ for an altitude below 11 [km] is calculated from the measured static pressure (ISO standard atmosphere).

2.1.5 Resultant Force and Resultant Moment

At the end of a data compatibility check the resultant force $\underline{R} = \underline{R}^A + \underline{R}^F$ is calculated using Equ. (4) from

$$\frac{\partial(m \cdot \underline{V}_{Kg})}{\partial t} = \underline{\underline{M}}_{gb} \cdot (\underline{R}_b^A + \underline{R}_b^F) \quad . \tag{33}$$

Thus the resultant force in body axis system can be calculated by

$$\underline{R}_b = m \cdot \underline{\underline{M}}_{bg} \frac{\partial \underline{V}_{Kg}}{\partial t} \quad . \tag{34}$$

The resultant moment can be obtained from

$$\frac{\partial (\underline{\underline{T}} \cdot \underline{\Omega}_b^{gb})}{\partial t} = (\underline{Q}_b^A + \underline{Q}_b^F) - \underline{\Omega}_b^{gb} \times (\underline{\underline{T}} \cdot \underline{\Omega}_b^{gb}) \quad . \tag{35}$$

With the inertia tensor of the aircraft

$$\underline{\underline{T}} = \begin{bmatrix} I_x & -I_{xy} & -I_{zx} \\ -I_{xy} & I_y & -I_{yz} \\ -I_{zx} & -I_{yz} & I_z \end{bmatrix} \tag{36}$$

the calculation of the resultant moment results in

$$\underline{Q}_b = \underline{\underline{T}} \cdot \frac{\partial \underline{\Omega}_b^{gb}}{\partial t} + \underline{\Omega}_b^{gb} \times (\underline{\underline{T}} \cdot \underline{\Omega}_b^{gb}) \quad . \tag{37}$$

The time derivatives of the angular velocities $\partial \underline{\Omega}_b^{gb} / \partial t = [\dot{p} \quad \dot{q} \quad \dot{r}]$ are determined numerically.

2.1.6 Inertia Data of the Aircraft

The mass of the aircraft 'm' and the position of the center of gravity are obtained from two three-point balances of the aircraft at different inclination angles before (or after) a flight test. On the ground the inclination angle of the aircraft is about ten degrees. If the rear is lifted other inclination angles up to zero degrees are feasible. The positional change of the center of gravity of the tanks (main tanks and especially the long additional tanks under the wings) as a function of the inclination angle and the filling of the tanks has to be taken into account.

The moments of inertia of the aircraft were estimated from bifilar pendulum tests / 13/. So far the moments of inertia are calculated as the difference between the current equipment and the test equipment used during the tests described in / 14/.

With these preparations the mass, the center of gravity and the moments of inertia of the aircraft are well known for the beginning (end) of a flight test. The additional knowledge of the fuel consumption during the flight test enables the calculation of the inertia data for the whole flight.

2.1.7 First Results of the Improved Data Compatibility Check

The results of the identification (Fig. 8, Fig. 9) are good despite the encountered large wind disturbances (wind speed about 40 [km/h], see Fig. 6). In addition to the wind field parameters (15 parameters of 30 are used) the initial values of the state variables (Φ_0, Θ_0, Ψ_0, $V_{GS,0}$, χ_0, $\dot{h}_0$, φ_0, λ_0, h_0) are estimated. For the measurement correction it is sufficient to take only the offsets Δa_x, Δa_y, Δa_z (about 10^{-5} [m/s^2]) and Δp_α =-0,277 [hPa] into account. The estimated form parameter from (31), (32) is b_1=2.17 (b_2 is set to zero) and the rotation angle (28) α_n=6.53 [°] (β_n is negligible small). Though the difference between measured and estimated Euler angles as well as measured and estimated position are so small that they are not visible only the estimation of the flight-path velocity and the aircraft velocity is presented.

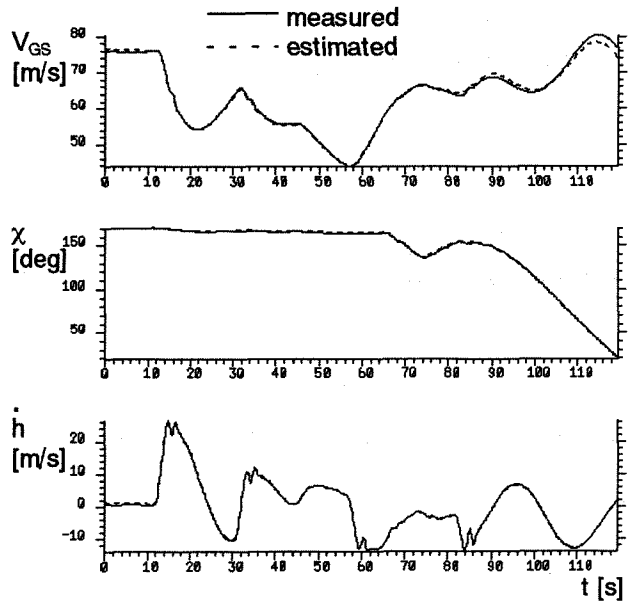

Fig. 8: The measured and estimated components of the flight-path velocity.

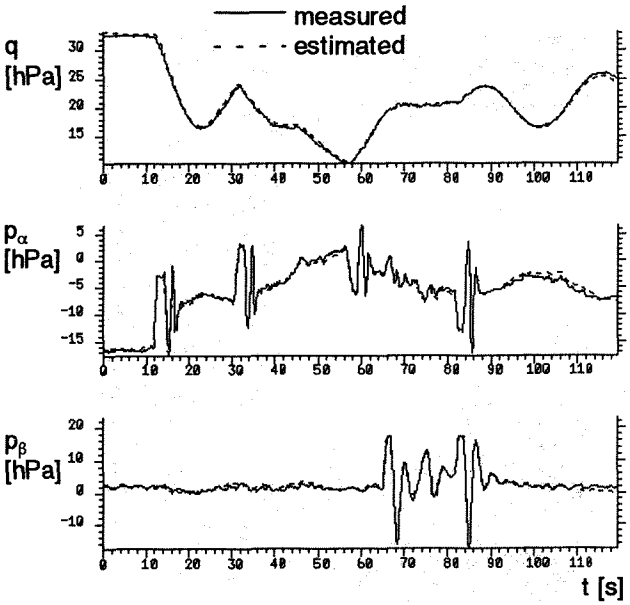

Fig. 9: Identification result of the aircraft velocity (raw data of the five hole probe) with the wind estimation according Fig. 6.

2.2 Aircraft Specific Model Part

One of the advantageous of the "Estimation Before Modeling" technique / 19/ is that the second part of the identification only requires the solution of algebraic equations. Thus the computational time can be reduced dramatically. From the input signals η, ζ, ξ, the aircraft velocity $\underline{V}_A$ and the shaft power P the resultant force and the resultant moment are estimated and compared with the corresponding quantities of the data compatibility check (Section 2.1.5).

The local observer discussed in Section 3.1 only requires the force equations of the aerodynamic and the propulsion system. The moment equations are not necessary for the design (of the observer) and will not be discussed in this paper.

2.2.1 The Force Equ. of the Aerodynamic Model

The aerodynamic force $\underline{R}^A$ in body-fixed coordinates is given by

$$\underline{R}_b^A = \underline{\underline{M}}_{ba} \cdot \bar{q} \cdot S \cdot \left[-C_D,\ C_Q,\ -C_L\right]_a^T$$

with the wing area S and the drag coefficient C_D

$$C_D = C_{D0} + (C_{D\alpha} + C_{D\alpha^2} \cdot \alpha) \cdot \alpha + (C_{D\beta} + C_{D\beta^2} \cdot |\beta|) \cdot |\beta| + C_{D\alpha\beta} \cdot \alpha \cdot \beta + C_{Dq} \cdot \frac{q \cdot l_\mu}{V_A} + f(\dot{\alpha}, \dot{\beta}, \eta, \eta_K, \ldots) \quad (38)$$

the side force coefficient C_Q (s is half of the wing span)

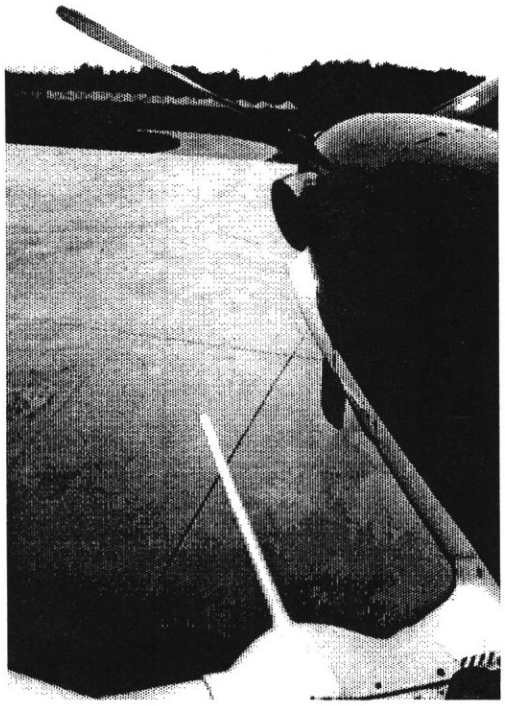

Fig. 10: The Pitot Tube behind the right propeller.

$$C_Q = C_{Q\beta} \cdot \beta + C_{Q\zeta} \cdot \zeta + (C_{Qp} \cdot p + C_{Qr} \cdot r) \cdot \frac{s}{V_A} + C_{Q\alpha\beta} \cdot \alpha \cdot \beta + f(\dot{\beta}, \xi, \ldots) \quad (39)$$

and the lift coefficient C_L

$$C_L = C_{L0} + (C_{L\alpha} + C_{L\alpha^2} \cdot \alpha) \cdot \alpha + (C_{L\beta} + C_{L\beta^2} \cdot |\beta|) \cdot |\beta| + C_{L\alpha\beta} \cdot \alpha \cdot \beta + C_{Lq} \cdot \frac{q \cdot l_\mu}{V_A} + f(\dot{\alpha}, \dot{\beta}, \eta, \eta_K, \ldots) \quad (40)$$

The Equ. (38) through (40) describe a one point aerodynamic model where the effects of the wing, the fuselage and the elevator as well as the rudder are combined. For cruise flight conditions and low dynamic maneuvers the accuracy of this model should meet the requirements of the observer. For high dynamic maneuvers more complex models (multi-point models) are available. The secondary effects mentioned in brackets at the end of the equations are neglected.

2.2.2 The Propeller Model

The propeller force $\underline{R}^F$ can be expressed as

$$\underline{R}_b^F = \frac{P}{V_A} \cdot \eta_{Prop} \cdot \left[\cos\sigma,\ 0,\ \sin\sigma\right]^T \quad (41)$$

where σ is the angle between the x-axis of the airplane and of the propeller axis (for the DO128 σ=-2 [°]). In this equation the term $(P/V_A) \cdot \eta_{Prop}$ represents the thrust F. The propeller efficiency η_{Prop} is given by the propeller charts of the manufacturer as a function of airspeed, air density and speed of the propeller. The deterioration of the propeller efficiency caused by the installation of the propeller (e.g., by drag in the propeller flow) is neglected. The propeller charts are valid for axial flow. A valuation of the effects by non-axial flow gave the following results. For a typical airspeed of 67m/s and an inclination angle δ of ten degrees

$$\delta = \arccos(\cos\beta \cdot \cos(\alpha + \sigma)) \quad (42)$$

the axial thrust increases from 3300 [N] to 3344 [N] (1.3%) for a constant blade angle. This effect is negligible but in addition the non-axial flow causes a propeller side force of about 380 [N] and a moment $M_{z,prop}$ of 429 [Nm].

2.2.3 Additional Observation Equations

As mentioned above it is planed to improve the accuracy of the identified model by additional measurements.

2.2.3.1 The Pitot Tube

The already mentioned PITOT tube behind the propeller is integrated into the flight test equipment (Fig. 10).

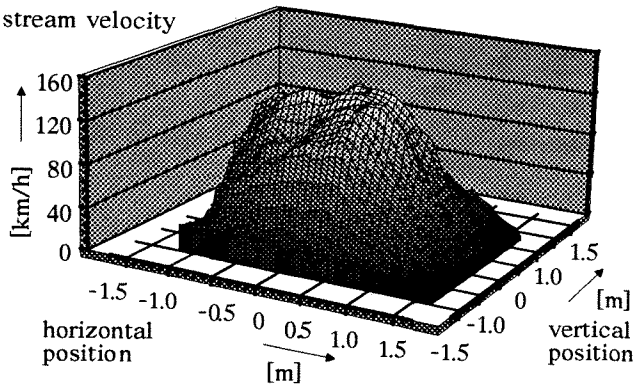

Fig. 11: Measured stream velocity (F=2490.9N).

This sensor in the propeller area measures the air pressure and allows to determine the stream velocity at this location. Though an additional measurement of the radial pressure distribution in the propeller area in a ground test (Fig. 11) the accompanying distribution for axial stream is known. This distribution can be used for the calculation of the effect of the propeller flow on the wing (Section 2.2.3.2).

The Pitot tube has a second function. The integration of the pressure over the whole propeller area (measured in ground tests) leads to the propeller thrust valid for the airplane at rest and for axial stream conditions. Fig. 12 shows this calculated thrust as a function of the pressure measured by the PITOT tube.

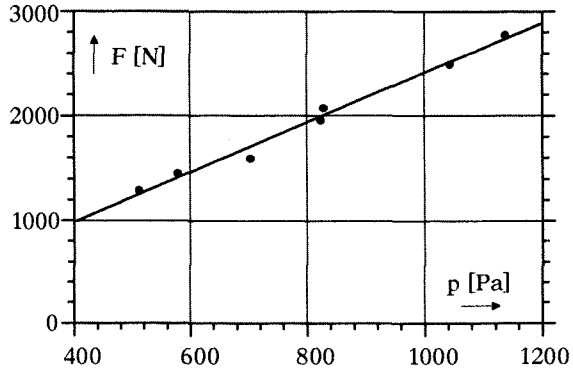

Fig. 12: Thrust F as a function of Pitot pressure.

2.2.3.2 *Measurement of the Wing Pressure*

It is planned to use the measured wing pressure to support the estimation of the lift in several wing sections. The wing section behind the propeller for example allows one to estimate the effect of the propeller stream velocity on the wing.

The measurement of the wing pressure distribution over the whole airfoil allows to determine the lift coefficient. The geometry of the measured pressure distribution for different angles of attack should be similar. Thus the measurement of the pressure at one point x/c is a linear function of the lift coefficient C_l even through high angles of attack. The measured pressure distribution (wind tunnel test data) of the airfoil NACA 23018 / 20/ (airfoil of the DO128) results in the following illustration (Fig. 13).

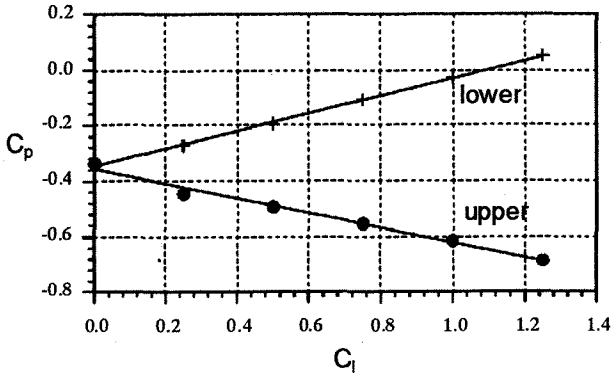

Fig. 13: Pressure coefficient C_p at x/c=0.49 for the airfoil NACA 23018 from wind tunnel test data published in / 20/.

The differential pressure sensors mounted in the wing of the DO128 measure the pressure between one point of the wing p_w and the static pressure p_s. Thus the pressure coefficient can easily be obtained by

$$C_P = \frac{p_w - p_s}{\bar{q}} \quad . \tag{43}$$

It is desirable to measure the wing pressure in the vicinity of the nose, if possible in the first third of the airfoil. But it is impossible to measure the wing pressure there due to the de-icing system and the spar of the wing. A feasible mounting position closest to the nose of the airfoil is at x/c=0.49. This results in a turbulent stream at the upper surface pressure holes, starting at smaller angle of attack. For higher angles of attack the turbulence destroys the linear relationship between determined pressures and the lift coefficient.

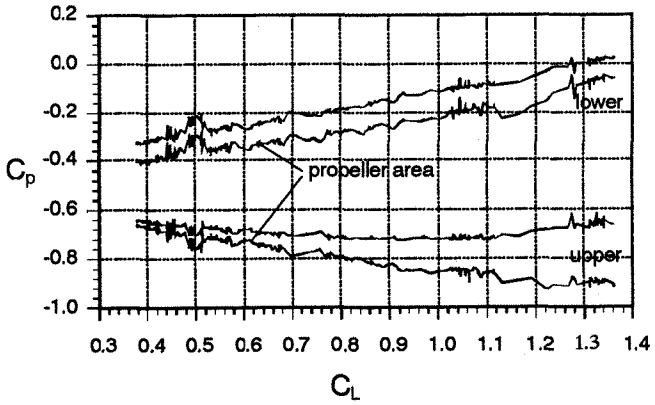

Fig. 14: Preliminary results of the wing pressure measurements.

Due to defective pressure sensors the crucial series of flight tests had to be repeated in April 1994. The following discussion is based on a preliminary evaluation of this new flight data. The final results of the ongoing evaluation are expected to be available for the presentation.

In Fig. 14 the first evaluation of the flight test data is shown for an uninterrupted four minutes part of the flight. The lift coefficient C_L of the aircraft is calculated by

$$C_L = \frac{m \cdot g}{\bar{q} \cdot S} \quad . \tag{44}$$

This equation is a simple approximation valid for horizontal flight. The disturbances in Fig. 14 arise from strong aircraft maneuvers (curves) where Equ. (45) is not valid. The differences compared to Fig. 13 and the differences between the two wing sections are due to the fact that C_L is an approximation of the lift coefficient of the whole aircraft and not for the examined wing sections.

In the ongoing evaluation the wing is divided into several wing sections. For each section the lift is calculated separately from the local airspeed velocity (calculation similar to Equ. (24), in addition the induced angle of attack α_i has to be taken into account) and from the local lift coefficient. The local lift coefficient is a linear function of the local pressure coefficient (see Fig. 13) and the pressure coefficient is given by Equ. (44).

3 Observer

This section discusses two methods for sensor supervision of a five hole probe. The supervision is based on accurately measurable output variables of the aircraft, particularly the outputs of the laser strapdown platform. The problems associated with both methods as well as the advantageous of both methods are outlined / 4/.

3.1 The Nonlinear Local Luenberger Observer

The model implemented in the observer is just a part of the complex six-degrees-of-freedom aircraft model / 7/. To avoid model parameters whose values are inaccurately known as well as to reduce the computational requirements for the later on-line calculation, the moment equations are replaced by precisely measured data, namely $\underline{\Omega}$, $\underline{\Phi}$ (local observer, / 9/). The acceleration as a fast and accurate measurement is chosen here to compare the output of the observer $\underline{\hat{a}}$ with the corresponding measurement $\underline{a}$. The difference (estimation error $\underline{\tilde{a}}$) is fed back through the diagonal matrix $\underline{\underline{H}}$ to the integrator inputs of the observer. The coefficients of this matrix have an influence on the stability, the low-pass filter effect and the response time of the observer.

Since this observer is insensitive to wind disturbances the wind is neglected ($\underline{\hat{V}}_W = \underline{0}$) in the observer model. Translational wind does not have any effect on the stationary estimation error of the observer / 3/.

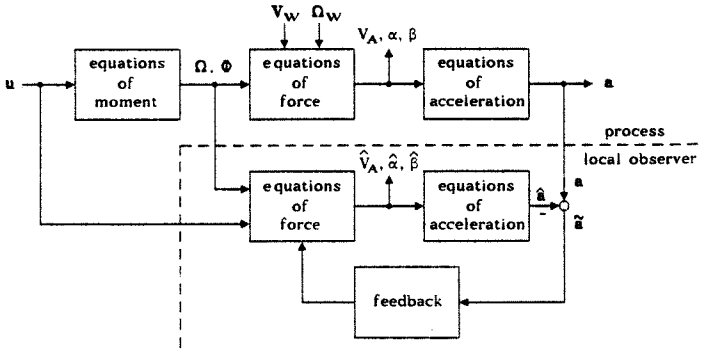

Fig. 15: The local Luenberger observer / 7/.

The observer based on this concept is able to estimate the aircraft velocity in polar coordinates V_A, α, β. Since on board the aircraft these components are now measured by the five hole probe, the observer is extended by the equations in Section 2.1.4.3 to estimate the pressures measured by this sensor. In addition the variation of the parameters can be dramatically reduced by the improved model equations presented in Section 2. The first results of the data compatibility check in Section 2.1.7 indicate that the needed measurement corrections are now minimal. Thus the estimation results of the redesigned observer should satisfy the required estimation accuracy (see Section 1). More detailed results will be presented at the conference.

3.2 Recursive Equation Solver

The direct inversion is a second possibility to calculate/estimate the measurements of the aircraft velocity. It uses the complex nonlinear relationship between the measured acceleration $\underline{a}_b^{ib}$ and the aircraft velocity $\underline{V}_A$ respective the pressures of the five hole probe. For the solution of this set of equations an analytical inversion is not completely feasible. Therefore, a very efficient inversion algorithm is needed.

One of the disadvantages of direct inversion algorithms is that one has to rely on the fast and safe convergence of the available programs. Convergence is not guaranteed and the computational times of the algorithms are not constant / 4/. In addition high frequency disturbance (noise) are not filtered out.

The advantage of the direct inversion is that there is no delay at the start. So the direct inversion might be useful for generating start values for an observer / 4/.

4 Summary and Conclusion

The additional measurement signals available from DGPS, PITOT tube (mounted behind the propeller) and wing pressure sensors allow to improve both the aircraft model as well as the model of the measurement system. In the off-line identification additional measurement equations containing further unknown parameters are introduced. The introduced uncertainties can be reduced by additional information obtained from ground tests of the propeller and from wind tunnel test data of the airfoil.

The improved model with less variant parameters is the base for the implementation of analytic and dissimilar redundancy. Therefore the design of a nonlinear observer and a recursive equation solver for generation of start values is outlined.

References

/ 1/ Brockhaus, R., A mathematical multi-point model for aircraft motion in moving air. Zeitschrift für Flugwissenschaft und Weltraumforschung, 11, 174 - 184., 1987.

/ 2/ Brockhaus, R., Flugregelung, Springer, Berlin, Heidelberg, New York, 1994.

/ 3/ Buchholz, J.J., Sensor Fault Detection and Analytic Redundancy by Means of Deterministic Observers. Third International Symposium on Aviation and Space Safety, p. 181 - 189, Toulouse, 1988.

/ 4/ Buchholz, J.J., Observer or Direct Inversion. AIMS, RWTH Aachen, 1989.

/ 5/ Buchholz, J.J., Polynomial Classifiers for Sensor Fault Detection. Technical Diagnosis, Helsinki, 1990.

/ 6/ Doherr, K.-F., Weiß, S., Ein 1-parametriges Modell für halbkugelförmige Fünflochsonden (A Single-Parameter Model for Hemispherical Five Hole Probes). Zeitschrift für Flugwissenschaft und Weltraumforschung, Vol. 14, No. 3, p. 193 - 198, 1990.

/ 7/ Dunkel, W., Buchholz J.J., Validation of a Model for a Nonlinear Local Luenberger Observer Using Measured Data. Second Braunschweig Aerospace Symposium, Braunschweig, 1990.

/ 8/ Dunkel, W., Identification of a Nonlinear Model for State Estimation in an Airplane. IFAC/IFORS Symposium, Budapest, 1991.

/ 9/ Dunkel, W., Brockhaus, R., A Nonlinear Observer for Sensor Fault Detection in an Airplane. IFAC/IMACS Symposium, BadenBaden, 1991.

/ 10/ Dunkel, W., An Improved Model of a Propeller Aircraft. IMACS Symposium 1.Mathmod Vienna, p. 918, Wien, 1994.

/ 11/ Gertler, J., Analytical Redundancy Methods in Fault Detection and Isolation. IFAC/IMACS Symposium, BadenBaden, 1991.

/ 12/ Göllinger, H., Model Extensions for Describing Properties of a Flight Test Measurement System. IMACS Symposium 1.Mathmod Vienna, p. 484, Wien, 1994.

/ 13/ van Hemel, J.J.O., Mulder, J.A., Proskawetz, K.O., Estimation of Aircraft Inertia Characteristics from Bifilar Pendulum Test Data. Zeitschrift für Flugwissenschaft und Weltraumforschung, Vol. 17, No. 1, p. 45 - 51, 1993.

/ 14/ Jategaonkar, R., Identification of the Aerodynamic Model of the DLR Research Aircraft ATTAS from Flight Test Data. DLR-FB90-40, Braunschweig, July 1990.

/ 15/ Jategaonkar, R., Determination of Aerodynamic Characteristics from ATTAS Flight Data Gathering for Ground-Based Simulator. DLR-FB91-15, Braunschweig, May 1991.

/ 16/ Laban, M., Mulder, J.A., On-Line Identification of Aerodynamic Model Parameters. IFAC/IFORS Symposium, Budapest, 1991.

/ 17/ Press, W.H., Flannery, B.P., Teukolsky, S.A., Vetterling, W.T., Numerical Recipes. Cambridge University Press, Cambridge, 1986.

/ 18/ Proskawetz, K.O., Brockhaus, R., Flight Path Reconstruction a Powerful Tool for Data Compatibility Check. ICAS Congress ICAS865.4.4, London, 1986.

/ 19/ Proskawetz, K.O., Systemidentification of airplanes using the „Estimation Before Modeling" Technique. Z. Flugwissenschaft und Weltraumforschung, 15, 401407, 1991.

/ 20/ Riegels, F.W., Aerodynamische Profile, München, 1958.

/ 21/ Vörsmann, P., An On-Line Realization for Precise Wind Vector Measurements on Board the DO28 Research Aircraft. ICAS-84-5.10.1, Toulouse, 1984.

/ 22/ Wei, W., Proskawetz, K.O., ML-Data-Compatibility-Check of General Flight-Test-Data By Use of a Nonlinear Six Degrees of Freedom Model. IFAC/IFORS Symposium, Beijing, Aug. 1988.

/ 23/ Yuan, J., Schänzer G., Gu. X., Jacob, Th., Error correction for Differential GPS with long separated ground station and user for aircraft landing. Proc. of 2. Intern. Symp. on Precise Positioning with GPS, Ottawa, 1990.

/ 24/ Department of Defense World Geodetic System 1984, DMA Technical Report 8350.2, 1987.